Impact of doubled CO_2 on the interaction between the global and regional water cycles in four study regions

Zhao Li · Uma S. Bhatt · Nicole Mölders

Abstract Results from a suite of 30-year simulations (after spin-up) of the fully coupled Community Climate System Model version 2.0.1 are analyzed to examine the impact of doubling CO_2 on interactions between the global water cycle and the regional water cycles of four similar-size, but hydrologically and thermally different study regions (the Yukon, Ob, St Lawrence, and Colorado river basins and their adjacent land). A heuristic evaluation based on published climatological data shows that the model generally produces acceptable results for the control $1\times CO_2$ concentration, except for mountainous regions where it performs like other modern climate models. After doubling CO_2, the Northern Hemisphere receives significantly (95% confidence level) more moisture from the Southern Hemisphere during the boreal summer than under $1\times CO_2$ conditions, and the phase of the annual cycle of net moisture transport to areas north of 60°N shifts to a month later than in the reference simulation. Precipitation and evapotranspiration in the doubled CO_2 simulation increase for the Yukon, Ob, and St Lawrence, but decrease, on average, for the Colorado region compared to the reference simulation. For all regions, interaction between global and regional water cycles increases under doubled CO_2, because the amount of moisture entering and leaving the regions increases in the warmer climate. The degree of change in this interaction depends on region and season, and is related to slight shifts in the position/strength of semi-permanent highs and lows for the Yukon, Ob, and St Lawrence; in the Colorado region, higher temperatures associated with doubling CO_2 and the anticyclone located over the region increase the persistence of dry conditions.

1 Introduction

In recent years, discussions of global warming and occurrence of intense local floods and droughts have heightened public awareness of the potential relationship between increased CO_2 concentrations and altered regional water cycles. Recent studies reported a twentieth century global average surface-temperature increase of about 0.6 K, or 0.07 K decade^{-1} (e.g., Peterson and Vose 1997; Folland et al. 2001); since 1976, that average has increased to about 0.15 K decade^{-1} (e.g., Houghton et al. 2001). The temperature increase is attributed to substantially increased CO_2 concentration, from about 280 ppm in 1800 to 355 ppm in 1990, in response to the industrial revolution and increasing world population (e.g., Houghton et al. 2001; Wang et al. 2004). General circulation models (GCMs) predict that temperature changes associated with global warming may be greatest at high latitudes (e.g., Giorgi et al. 2001). The high latitudes are a particularly sensitive global water cycle component due to feedbacks such as decreased albedo from reduced snow cover, or to the impact of increased melt-water on Arctic freshwater fluxes and, hence, thermohaline circulation (e.g., Broecker 1997). Thus, the high latitude hydrological cycle is extremely sensitive to global warming.

During the last century, global precipitation increased by 2% (e.g., Jones and Hulme 1996; Hulme et al. 1998), while mid- and high-latitude precipitation increased about 7–12% (e.g., Houghton et al. 2001). For increasing CO_2

Z. Li · U. S. Bhatt · N. Mölders (✉)
Geophysical Institute and
College of Natural Sciences
and Mathematics, Atmospheric Science Program,
University of Alaska Fairbanks, 903 Koyukuk Drive,
P.O. Box 757320, Fairbanks, AK 99775-7320, USA
e-mail: molders@gi.alaska.edu

conditions further precipitation changes have to be expected; the United Kingdom Meteorological Office High Resolution 11-level GCM and the Australian Commonwealth Scientific and Industrial Research Organization 9-level GCM, both produced an increase (decrease) in the number of wet days at high-latitudes (mid-latitudes) for a doubled CO_2 scenario (e.g., Hennessey et al. 1997).

Due to complex interactions between energy and water cycles, increasing CO_2 concentrations and temperatures affect water cycling at different temporal and spatial scales. Therefore, it is important to examine water cycles and their interactions at different scales. "Global water cycle" refers to a closed system of water circulation encompassing evaporation from oceans, large-scale atmospheric transport, precipitation over land and water, and runoff back to the oceans. "Regional water cycle" refers to large-scale atmospheric transport of water substances and runoff into and out of a sub-global domain, plus precipitation and evapotranspiration (sum of evaporation, transpiration, and sublimation) within the domain. A fraction of the precipitation may stem from previous precipitation within the domain; a fraction of the evapotranspiration may contribute to moisture export (e.g., Eltahir and Bras 1996). Interactions between the global water cycle and a regional water cycle consist of water substances flowing into and out of the region. Thus, we define "interaction between global and regional water cycles" as moisture flux over a region's lateral boundaries. This inflow and outflow determines the degree to which factors external to a region control that region's water cycle, i.e., the global water cycle's influence on the regional water cycle.

In this study, we examine the impact of the doubled-CO_2 greenhouse scenario to elucidate interactions of the global water cycle with regional water cycles in four similarly sized, but hydro-thermally different regions. To this end, we run the Community Climate System Model (CCSM) version 2.0.1 (e.g., Blackmon et al. 2001; Kiehl and Gent 2004) assuming $1\times CO_2$ and $2\times CO_2$ concentrations, and analyze model output for 30 years after spin-up. We explore the mechanisms driving the regional water cycles, highlight their interactions with the global water cycle, identify global and regional changes in the water cycles and their interactions, and elaborate causal mechanisms. Furthermore, we investigate whether the mechanisms, interactions, and changes in response to doubling CO_2 are region-specific.

2 Experimental design

2.1 Model description

The CCSM modeling suite (e.g., Blackmon et al. 2001; Kiehl and Gent 2004) consists of the Climate Atmosphere

Model (CAM) version 2, the Common Land Model (CLM) version 2, the Parallel Ocean Program (POP), the Community Sea Ice Model version 4.0.1 (CSIM), and the flux coupler version 5.0.1. The flux coupler consistently exchanges data between model components without using flux corrections.

The CAM is an improved version of the Atmosphere General Circulation Model: Community Climate Model version 3 (AGCM: CCM3). It uses hybrid vertical coordinates with a terrain-following σ-coordinate starting at the surface that smoothly transitions into pressure coordinates around 100 hPa. The major differences between CAM and CCM3 are the formulations for cloud condensed water, cloud fraction and overlap, and long-wave absorptivity and emissivity of water vapor (Kiehl and Gent 2004). Deep convection is simulated by a plume-ensemble approach; convective available potential energy (CAPE) is removed from a grid-column at an exponential rate based on Zhang and McFarlane (1995). Interaction between local convection and large-scale dynamics is considered through pressure field perturbations caused by cloud momentum transport (Zhang et al. 1998). Shallow convection is addressed following Hack (1994) and Zhang et al. (1998). At the resolvable scale, "non-convective" precipitation is calculated by parameterizing both macroscale processes that describe water-vapor condensation and associated temperature change, and microscale processes controlling condensate evaporation and condensate conversion to precipitation. Cloud microphysical processes are considered in accord with Rasch and Kristjánsson (1998). Grid-cell mean "non-convective" precipitation is obtained by integrating from the bottom to the top of the model (e.g., Rasch and Kristjánsson 1998; Zhang et al. 2003).

The CLM (Dai et al. 2003) is a successor of the National Center for Atmospheric Research Climate System Model's land surface model (Bonan 1998). Major improvements include considering land-cover spatial heterogeneity by explicitly dividing every grid cell into four land-cover types (glacier, lake, wetland, and vegetation). Vegetation is further divided into dominant and secondary plant functional type. The CLM considers ten layers for soil temperature, soil water, and ice content, and up to five snow layers, depending on snow depth.

The Los Alamos National Laboratory's POP (Smith et al. 1992) is used to simulate ocean processes. Major advantages of this model for our study include a North Pole displaced from the Arctic Ocean to Greenland (no filtering of the ocean solution is needed for the Arctic) and the fine resolution ($<1°$) that leaves the Bering Strait and Northwest passage open to permit simulation of the Arctic halocline (Holland 2003).

The CSIM (Briegleb et al. 2004; Holland et al. 2006) includes a sub-grid scale ice thickness distribution

parameterization. This parameterization considers five ice categories; each category occupies a fractional area within a grid cell. Compared to other sea-ice models without such a sea-ice thickness scheme, CSIM can represent a more extensive and thicker ice cover, and therefore better simulates the thermodynamic processes over the Arctic Ocean. This feature allows the simulation of more realistic ice-albedo feedback when CO_2 concentration doubles.

2.2 Simulations and study regions

CCSM is run in fully coupled mode with 26 vertical layers at a spectral truncation of T42, corresponding to a horizontal spatial resolution of $\approx 2.8 \times 2.8°$latitude/longitude. Simulations assuming CO_2 concentrations of 355 ppm (control, CTR) and 710 ppm (experiment, DBL) are performed for 40 years.

Each model component is equilibrated in offline mode. Both simulations start from the same equilibrated initial and astrophysical conditions for 01-01-1990. Since doubling CO_2 slightly disturbs the equilibrium of the conditions in the various compartments, the first 10 years are discarded as spin-up time to permit a new equilibrium to be achieved (Fig. 1).

We analyze the 30 years after the 10-year spin-up with special focus on four similar-size ($\approx 3.27 \times 10^6$ km^2) study regions, the Yukon, Ob, St Lawrence, and Colorado river basins and adjacent land (Fig. 2a), chosen for their contrasting hydrologic and thermal regimes. Although the Yukon and Ob both span the Arctic and the Subarctic, the Yukon is mainly characterized by cold permafrost in complex terrain, surrounded by oceans to the north, west, and south; the Ob is dominated by warm permafrost in relatively flat terrain with ocean to the north. The St Lawrence has a humid climate and moderate terrain; the

Great Lakes lie to the north and the Atlantic Ocean to the east. The Colorado has mainly a semi-arid climate and mountainous terrain, bordered by the Pacific Ocean on the west, and the Gulf of Mexico to the south.

2.3 Analysis

Results are analyzed with respect to changes in the 30-year annual, seasonal, and monthly averages of water-cycle-relevant fluxes (precipitation, evapotranspiration, runoff, and moisture fluxes through the lateral study-region boundaries), soil moisture, and residence time (ratio of average precipitable water to average precipitation).

Global and regional water–cycle interactions in response to doubling CO_2 are evaluated using moisture (water vapor and liquid and solid atmospheric water) transport through lateral boundaries. When examining global water-cycle changes we focus particularly on meridional exchange between the hemispheres and the area north and south of the circle described by a line drawn around 60°N latitude.

A Student's t test and F-test are performed to assess changes in mean values and temporal and spatial variations, respectively. The term "significant" will only be applied if changes are statistically significant at the 95% or higher confidence level.

We also evaluate whether the impact of doubling CO_2 varies between study regions. Note that higher-latitude plots display slightly more spatial detail than lower-latitude plots since grid cell number increases with latitude and study regions are of approximately equal area. For confidence in our results we heuristically evaluate model climatology, and briefly review the main findings of evaluations performed by others.

3 Heuristic evaluation of model climatology

3.1 Global climatology

When compared to observed January and July climatologies (e.g., National Climatic Data Center 1987), CTR captures near-surface air temperature patterns well except over Greenland and eastern Siberia in January, where the temperature is overestimated by about 8 K. In all study regions, near-surface air temperatures are simulated acceptably within ±3 K except for Colorado in July. There, near-surface air temperature is overestimated by about 6 K because terrain elevation is less than 2,000 m lower in the model than the highest peaks in nature.

Simulated global annual precipitation (land only, Antarctica and Greenland excluded) is 2.4 mm day^{-1} compared to 2.3 mm day^{-1} from the Global Precipitation
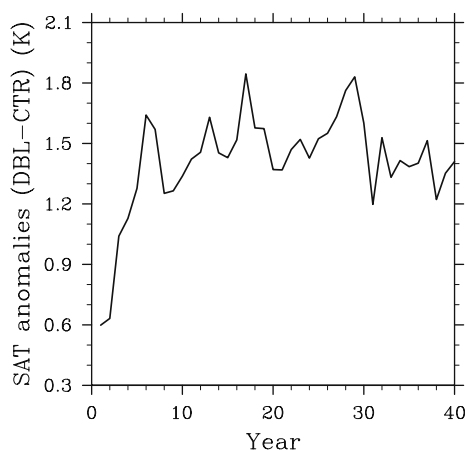

Fig. 1 Annual average near-surface air temperature (*SAT*) anomalies (DBL-CTR) used to determine spin-up time

Fig. 2 **a** GPCC precipitation climatology (1971–2000, land only) with the four study regions identified by boxes (from *left*: Yukon, Colorado, St Lawrence, and Ob). No long-term precipitation observations are available over the oceans, Greenland, or Antarctica. Note that the four regions are of similar area-size, but appear different on the displayed map due to the projection. **b** 30-year averaged annual precipitation (after spin-up) as obtained with CTR (land only). **c** Anomalies (DBL-CTR) of 30-year averaged annual precipitation; contour intervals are 60 mm year^{-1}: zero line is *bolded*, and positive and negative contours are shown in *solid* and *dashed lines*, respectively. *Shaded* areas indicate significant (95% confidence level or higher) changes
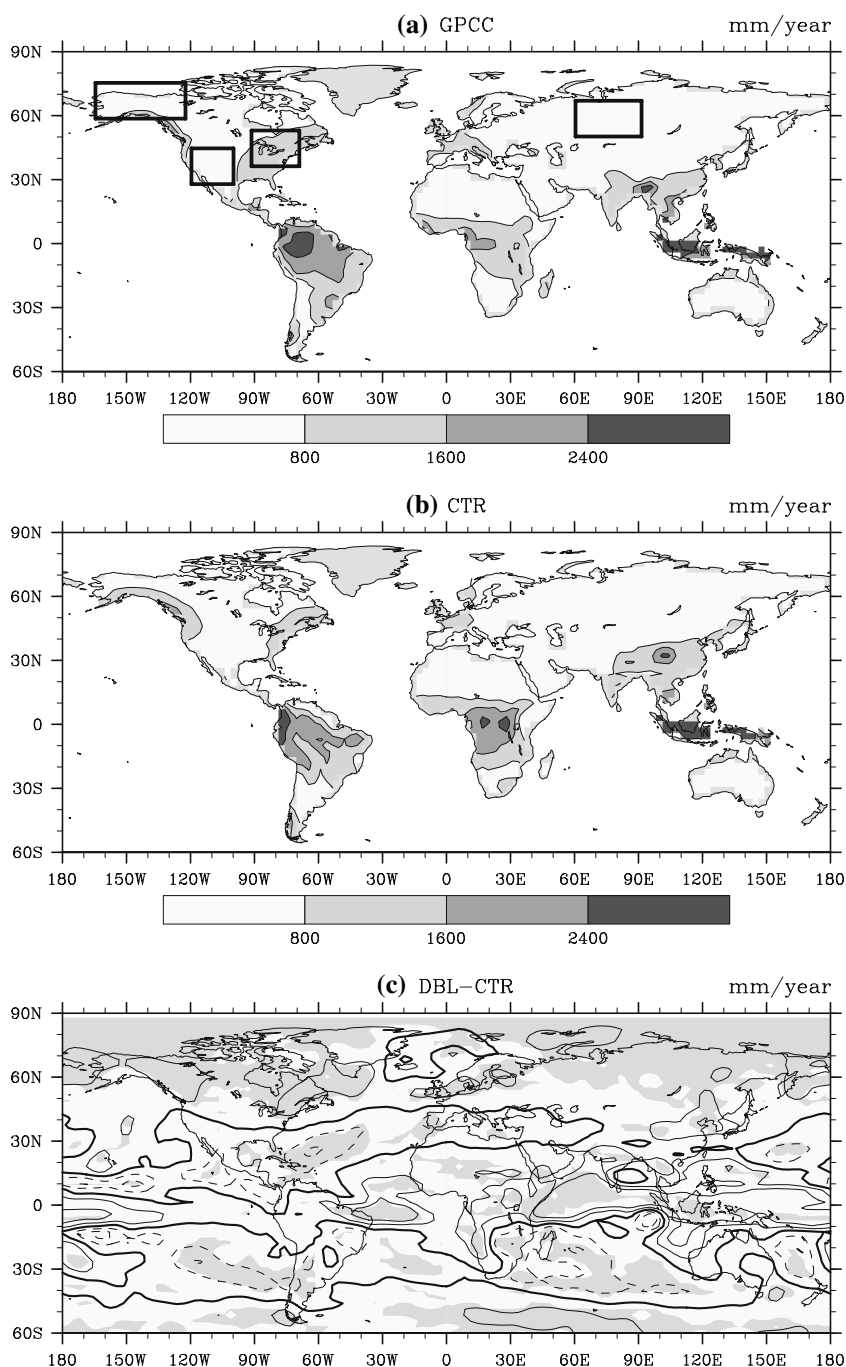
Climatology Center (GPCC) precipitation climatology. Simulated precipitation is 0.4 mm day^{-1} higher and hardly ($\approx$0.03 mm day^{-1}) lower than GPCC climatology in boreal winter and summer, respectively. The spatial correlation between the CTR and GPCC DJF (JJA) precipitation climatology (Fig. 2a, b) is 0.840 (0.699), i.e., in the same accepted performance range as other GCMs. For example, according to Program for Climate Model Diagnosis and Intercomparison (PCMDI) reports (Meehl et al. 2000; Covey et al. 2003) which compared precipitation predicted by 18 coupled GCMs to observational data, differences between simulated and observed global annual precipitation range between –0.1 to +0.4 mm day^{-1}, and the pattern correlation between simulated and observed precipitation ranges between 0.7 and 0.9. Biases found in CCSM (precipitation overestimation, southward-shifted South Pacific convergence zone, excessive northern mid-latitude precipitation) are common in coupled GCMs (e.g., Johns et al. 1997; Meehl et al. 2000; Covey et al. 2003; Furevik et al. 2003).

Evapotranspiration is governed by atmospheric (wind speed, water vapor deficit, temperature) and bio-geophysical conditions (e.g., vegetation type and fraction, soil type, water availability in the root space) (e.g., Milly 1991) and by how much water or snow is intercepted and stored by vegetation. The global distribution and magnitude of simulated evapotranspiration agrees well with published climatology derived from observations (e.g., Baumgartner and Reichel 1975; Oliver and Fairbridge 1987).

CTR predicts the largest annual runoff for the Indonesian Islands, Amazon, Congo and Yangtze basins, the St Lawrence region, and southeast Alaska, in good agreement with published runoff climatologies (e.g., Gregory and Walling 1973).

Permafrost soils are typically close to saturation (e.g., Hinkel et al. 2003). CTR predicts total soil volumetric water content (soil liquid water plus ice) close to saturation for permafrost areas (PanArctic, Greenland, Antarctica) in fall, spring, and winter. As expected, CTR also predicts high soil moisture in the Tropics and during late fall for storm-track regions.

3.2 Climatology of the study regions

For the Yukon, simulated precipitation ranges from less than 300 mm year^{-1} in the north to 1,400 mm year^{-1} in the southern coastal and mountainous terrain (Fig. 3a). Except for details related to differences between model and real-world terrain height, the simulated spatial precipitation distribution agrees well with GPCC climatology. The annual cycle of monthly average precipitation is acceptably captured, but monthly precipitation is systematically overestimated with larger differences in seasons with high likelihood of solid and convective precipitation (Fig. 4b). In the Arctic, catch deficits due to trace events or windy conditions can yield underestimates of >50% between measured and true precipitation (Førland and Hanssen-Bauer 2000). For example, annual average precipitation at Barrow, AK is 110.6 mm year^{-1}; trace precipitation occurs on 45–50% of annual precipitation days (Yang et al. 1998). This means that total annual observed precipitation amount may be larger than the 110.6 mm year^{-1} reported. The Yukon's coarse network and complex terrain also contribute to systematic differences. Taking these factors into account, the simulated precipitation is plausible.

For the Ob, annual precipitation gradually decreases towards the south in both simulated and GPCC climatology (Fig. 3b). CTR slightly overestimates (≤10 mm mon^{-1}) precipitation in all months except August and September (Fig. 4c). Terrain variation is moderate (standard deviation of terrain height is ±200 m); discrepancies mainly result from catch deficits and the coarse network.

For the St Lawrence, CTR accurately predicts monthly precipitation in the first 6 and last 2 months of the year, but it greatly underestimates precipitation (≤38 mm mon^{-1}) for July to October (Fig. 4d). This underestimation may relate to premature deep convection predicted by the convective scheme combined with CCSM's representation of the Great Lakes. During these months the warm Great Lakes provide favorable conditions for deep convection. CLM represents the Great Lakes as a subgrid-cell surface type (see Dai et al. 2003); the actual lake position and shoreline within the grid-cell are not considered.

On annual average, CTR acceptably captures annual precipitation gradient from the west to the Atlantic Ocean (Fig. 3c). In the southwest St Lawrence region, differences between actual and model land–sea distribution cause discrepancies in annual mean coastal precipitation.

In Colorado, the coarse observational network and substantial differences between modeled (≤2,000 m) and real-world (≤4,000 m) terrain elevation lead to large differences between simulated and observed climatology (Fig. 3d). Nevertheless, the main feature of low precipitation in the west gradually increasing to the east is evident. CCSM, however, fails to reproduce the annual cycle of observed precipitation (Fig. 4e). The difficulty of precipitation prediction over complex terrain is a well-known common problem of coupled GCMs (e.g., Johns et al. 1997; Flato et al. 2000; Coquard et al. 2004) and even mesoscale models (e.g., Colle et al. 2000; Narapusetty and Mölders 2005; Zhong et al. 2005). Comparison of simulated (15 coupled GCMs) to observed precipitation (Coquard et al. 2004) for the western United States, for instance, revealed that all models overpredict winter precipitation by as much as 2 mm day^{-1}, or even more. Particularly in mountainous areas, considerable discrepancies between simulated and observed summer precipitation are also found, with the averaged model bias ≈1.5 mm day^{-1}. The CCSM and GPCC climatologies differ by 0.6 and −0.2 mm day^{-1} for boreal summer and winter, respectively. Thus, CCSM performance in this particular area is better than the average performance of the major GCMs.

Compared to evapotranspiration climatologies (e.g., Baumgartner and Reichel 1975; Oliver and Fairbridge 1987), CTR acceptably reproduces the north-south gradient of Yukon evapotranspiration (Fig. 5a), overestimates annual central Ob evapotranspiration (Fig. 5b), and successfully captures the St Lawrence gradient in annual water supply to the atmosphere (Fig. 5c). For the Yukon, Ob, and St Lawrence, evapotranspiration is greatest in July (Fig. 6 b–d); in Colorado, maximum evapotranspiration occurs in May/June (Fig. 6e). The annual monthly averaged evapotranspiration cycle has a wider range for the St Lawrence and Ob than for the Yukon and Colorado regions. Compared to various climatologies (Croley et al. 1998; Su et al.

Fig. 3 GPCC precipitation climatology (*long dashes*) and 30-year averaged annual precipitation obtained with CTR (*solid line*) or DBL-CTR (*gray shades*) for the **a** Yukon, **b** Ob, **c** St Lawrence, and **d** Colorado regions. Note that *gray shades* use different spacing for Colorado than for the other regions to better illustrate the anomalies
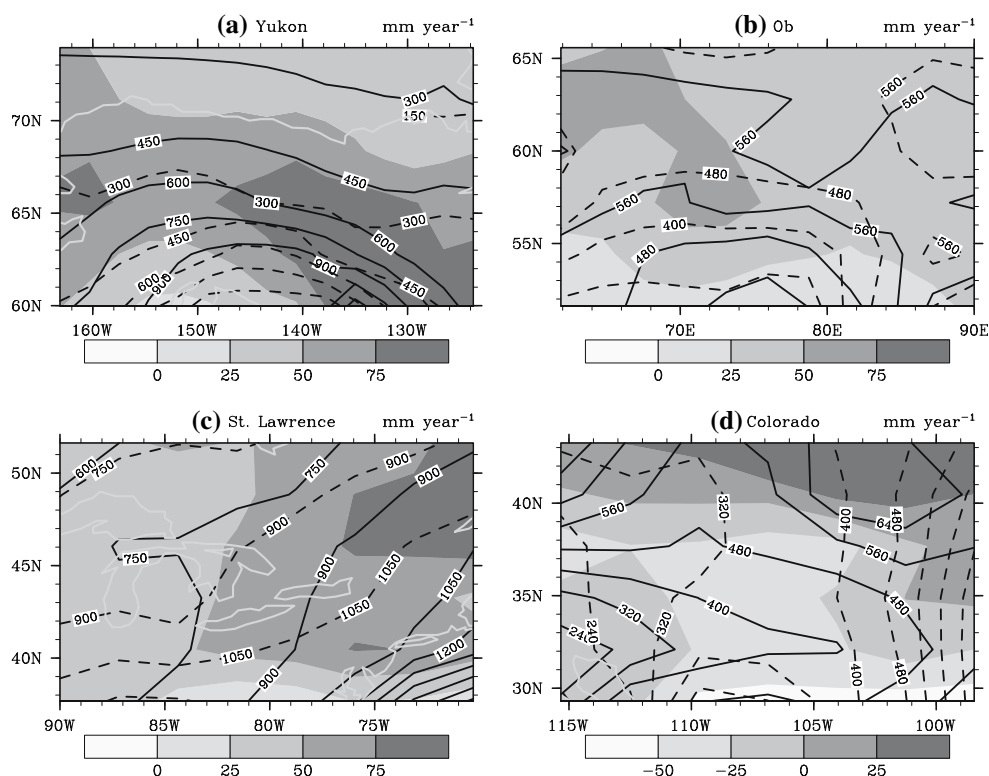
2006) and to European re-analysis 40 (ERA-40) data (Uppala et al. 2005), the pattern of the annual evapotranspiration cycle is captured acceptably in all study regions. Maximum evapotranspiration is overestimated by less than 1 mm day^{-1} at high-latitudes, and underestimated by less than 1.5 mm day^{-1} in mid-latitude study regions.

Both observed and modeled runoff is closely correlated ($R > 0.604$) with spring snowmelt for the Yukon, Ob, and St Lawrence; for the Colorado, precipitation-driven runoff is maximum in winter and minimum in late summer (Fig. 7e). Minimum runoff is of similar magnitude for all regions, but occurs in winter for Yukon and Ob and in summer for St Lawrence and Colorado. For the Yukon, St Lawrence, and Colorado, CCSM captures annual runoff cycles acceptably compared to the climatology from Bonan et al. (2002). Maximum Ob runoff is predicted a month too early, compared to climatology.

Annual average volumetric water content and soil-moisture fraction (ratio of actual volumetric water content to porosity) integrated over the entire soil column are greatest in the Ob region, followed by the Yukon, St Lawrence, and Colorado region (Table 1). This means Colorado has much drier soils than do the other three regions. Over the annual cycle, monthly averaged volumetric water content integrated over the entire soil column varies least in the Yukon, followed by the Colorado, Ob and St Lawrence region (Table 1).

3.3 Discussion

The reasons for discrepancies between simulated and GPCC precipitation climatology (Figs. 2c, 3, 4) are manifold. First, interpolation from point measurements to the GPCC gridded ($2.5° \times 2.5°$) precipitation values introduces errors in areas of sparse data, in complex terrain, and by including redundant information from near-by sites (e.g., Dingman 1994). Grid resolution significantly affects precipitation bias (e.g., Frei and Schär 1998; Colle et al. 2000; Zhong et al. 2005), and the GPCC data must be interpolated to the $2.8° \times 2.8°$ CCSM grid. Second, average terrain height within a model grid-cell represents elevation; the highest simulated mountains are flatter than the highest natural peaks. Consequently, when moist air flows over a mountain barrier, saturation and precipitation formation occur later and farther downwind in the model than in nature; i.e., in the model, water vapor is supplied to the atmosphere by evapotranspiration and large-scale lifting rather than by forced lifting at the mountain barrier (e.g., Narapusetty and Mölders 2005). In addition, mountain precipitation sites do not represent large areas accurately (e.g., Frei and Schär 1998; Colle et al. 2000), so discrepancies between simulated and observed precipitation occur (Fig. 3a, d). Third, since cloud and precipitation formation are subgrid-scale processes for any GCM, they must be parameterized. CCSM, on average, overestimates

Fig. 4 Comparison of monthly averaged precipitation from CTR (*thick solid*), DBL (*thick dashed*), and GPCC (*thin dashed*) climatology for **a** continental areas over the globe, and for the land part of the **b** Yukon, **c** Ob, **d** St Lawrence, and **e** Colorado regions. Months with significant (95% confidence level or higher) increases are *circled*. Note that no precipitation observations are available over oceans, and *y*-axes differ for different regions
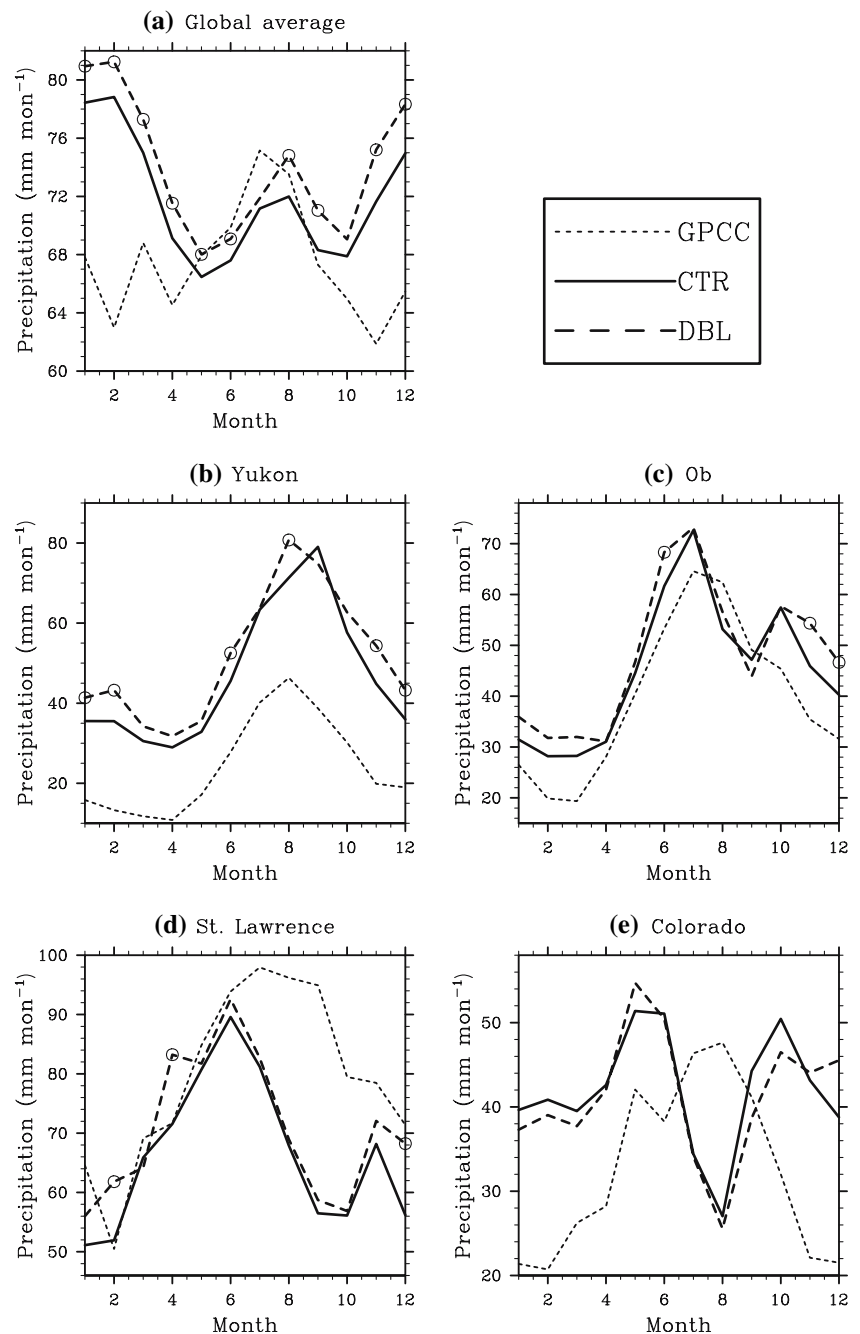
cloud-cover by 10–20% over land in northern mid- and high-latitudes in DJF compared to observed cloud climatology. CCSM predicts summertime rain too frequently at reduced intensity; because the predicted onset of daytime moist convection is about 4 h too early and the peak is too smooth (Dai and Trenberth 2004). Premature deep convection yields a ratio of convective to non-convective precipitation that is too high. Nevertheless, CCSM provides realistic patterns for precipitation >1 mm day^{-1} (Dai and Trenberth 2004). Fourth, it is well known that the coarse observational network is likely to miss thunderstorm events; underestimating observed precipitation causes lower predictive skill in summer. Fifth, splashing, catch deficits, occult precipitation, evaporation of collected precipitation, and trace precipitation (<0.1 mm day^{-1}) may result in values that are too low (Fig. 3a, b). For solid precipitation, for instance, catch deficiencies in snow measurements may be as large as 30% (e.g., Larson and Peck 1974; Yang and Woo 1999). Finally, differences between the actual coastline and that in the model may cause discrepancies between simulated and observed precipitation (Fig. 3a, c), because given the same temperature,

Fig. 5 30-year-averaged evapotranspiration (after spin-up) from CTR (in contour lines) for **a** Yukon, **b** Ob, **c** St Lawrence, and **d** Colorado. The anomalies (DBL-CTR) are shown by the *shaded field*. Note that *gray shades* use different spacing for Colorado than for the other regions to better illustrate the anomalies
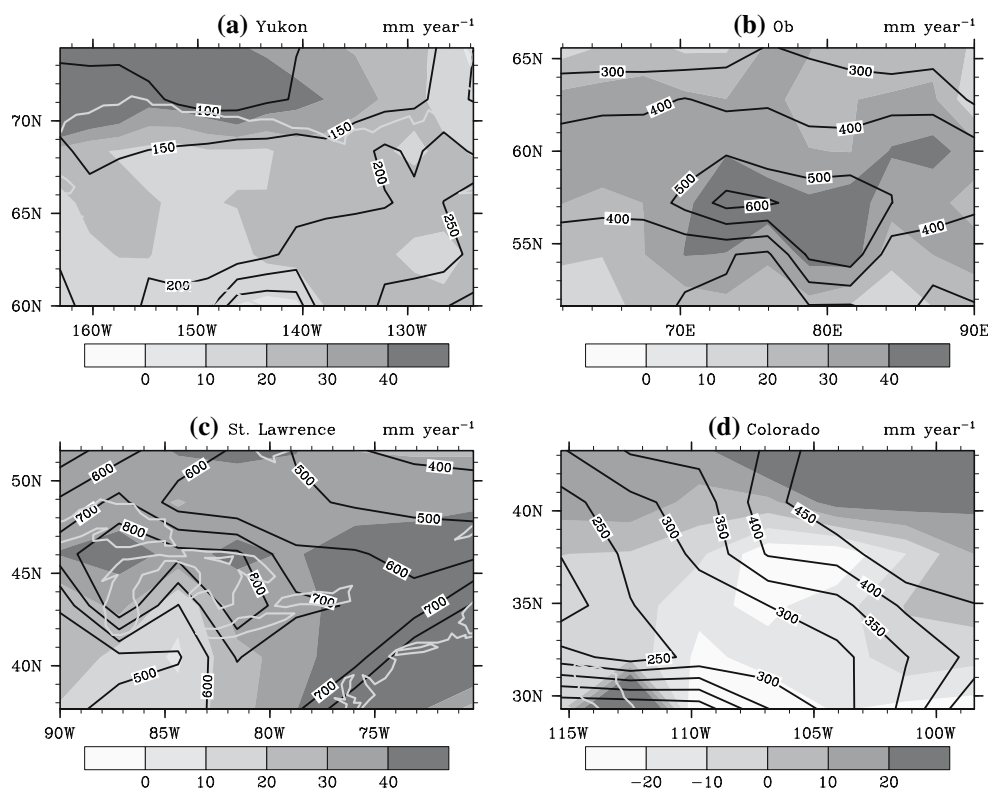
the water supply over water and land can differ greatly since evapotranspiration is bio-geophysically controlled.

Based on heuristic evaluations, CCSM produces reliable results for monthly and annually averaged water-cycle-relevant quantities on the global scale, and overall describes water-cycle-relevant processes well. CCSM captures regional-scale amount and spatial pattern of annually averaged values with sufficient accuracy. The main shortcoming (precipitation prediction over complex terrain) is common to most state-of-the-art coupled GCMs and mesoscale models (e.g., Johns et al. 1997; Colle et al. 2000; Flato et al. 2000; Coquard et al. 2004; Narapusetty and Mölders 2005; Zhong et al. 2005). In high altitude terrain, results may be more uncertain than in other regions, but the data represent current state-of-the-art modeling. However, because our interest here is to investigate water-cycle changes from CTR to DBL (i.e., differences), we assume that both simulations have similar deficiencies in mountainous terrain. Thus, one can conclude that CCSM is a suitable tool for examining the impact of doubling CO$_2$ on global and regional water cycle interactions.

## 4 Global water cycle changes

CCSM's climate sensitivity of 2.2 K in response to doubled CO$_2$ (Kiehl and Gent 2004) falls within the 1–3 K

climate-sensitivity range reported for other modern GCMs (e.g., Cubasch et al. 2001; AchutaRao et al. 2004). In response to doubling CO$_2$, air temperatures increase almost everywhere except around 60°S. Furthermore, globally averaged near-surface air temperatures increase 1.2 and 1.8 K in boreal summer and winter, respectively. These changes in response to doubling CO$_2$ agree with results from other GCMs (e.g., Mahfouf et al. 1994; Cubasch et al. 2001; AchutaRao et al. 2004). The greatest change occurs in high-latitude winter; the Arctic Ocean north of Europe shows the maximum increase of ≥8 K. In general, temperature increases more at high- than mid-latitudes because of ice/snow-albedo feedback (Fig. 8).

In DBL, annual evapotranspiration increases significantly north of 60°N except for most of Greenland. In the other regions, water supply to the atmosphere increases significantly in the Canada Basin of the Arctic Ocean, the US Southwest, and US East Coast in boreal winter and in most areas north of 50°N in boreal summer. Globally averaged evapotranspiration increases significantly in all months in DBL (Fig. 6a). Winter upper soil volumetric water content decreases (about 0.026 m^3 m^{-3}) over most of North America and Europe.

In DBL, annual-averaged residence time increases (1) globally, (2) in the Northern Hemisphere, (3) north of 60°N, and (4) for all four-study regions (Fig. 9; Table 2). In DBL, annual-averaged residence time increases <1 day

Fig. 6 Monthly averaged evapotranspiration from CTR (*solid*) and DBL (*dashed*) for **a** global average, and **b** Yukon, **c** Ob, **d** St Lawrence, and **e** Colorado regions. Note that *y*-axes differ
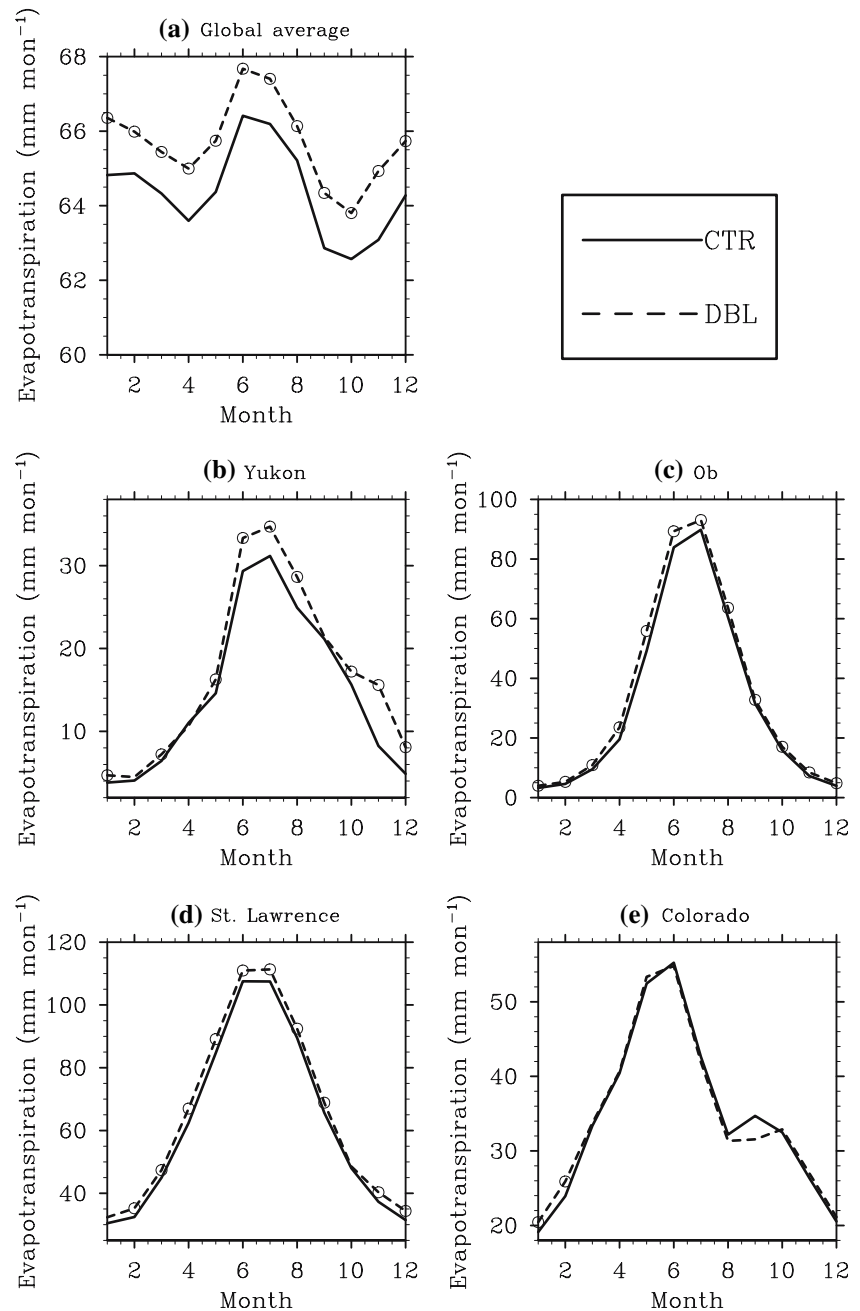
for most mid- and high-latitude regions; significant residence-time increases coincide with significant precipitation decreases for arid areas around 30°N and 30°S compared to CTR.

Global precipitation increases 2.4% ($\approx$0.8 mm day^{-1} for land area, excluding Greenland and Antarctica) in DBL compared to CTR. This increase is similar to increases shown by other model simulations (Meehl et al. 2000; Covey et al. 2003), especially when the wide range of precipitation variability is taken into account. Precipitation changes significantly in response to doubling CO$_2$ at high

latitudes and along the semi-permanent pressure-cell edges (Fig. 2c).

Doubling CO$_2$ significantly changes runoff in high latitudes and semi-arid areas. Annual runoff appreciably increases, for instance, in the Mackenzie and Lena, while it decreases, for instance, in the Ob and Colorado river basins. Globally averaged runoff increases slightly in most months, but significantly decreases in July (Fig. 7a), because the 1.3 mm mon^{-1} increase in globally averaged evapotranspiration is greater than the 0.7 mm mon^{-1} increase in precipitation.

Fig. 7 Monthly averaged
runoff as obtained from CTR
(*solid*) and DBL (*dashed*) for
a global average, and **b** Yukon,
c Ob, **d** St Lawrence, and
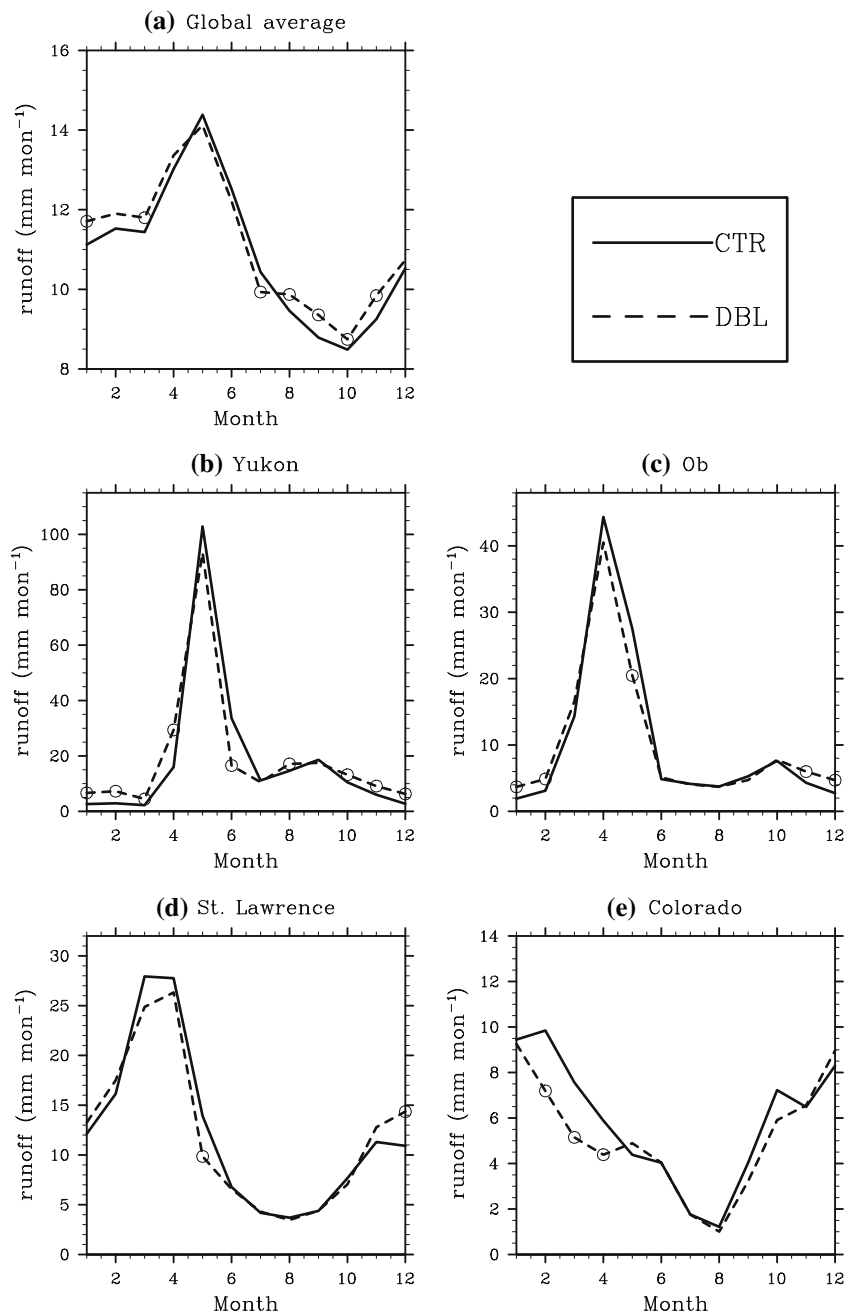**e** Colorado regions. Note that
y-axes differ

Table 1 Annual averages, minima and maxima of volumetric water content integrated over entire soil column and soil moisture fraction (ratio of actual volumetric water content to porosity) integrated over entire soil column

	Volumetric water content	Soil moisture fraction (%)	Minimum	Maximum
Yukon	0.294	68	0.268 (Jul)	0.310 (May)
Ob	0.380	86	0.350 (Aug)	0.402 (Mar)
St Lawrence	0.269	63	0.237 (Aug)	0.300 (Feb)
Colorado	0.177	41	0.152 (Aug)	0.201 (Jan)

The parentheses denote the month of occurrence

Fig. 8 30-year averaged near-surface air temperature (°C; after spin-up) obtained with CTR (in contour lines) for **a** Yukon, **b** Ob, **c** St Lawrence, and **c** Colorado. The anomalies (DBL-CTR; K) are shown by the *shaded field*. Note that *gray shades* use different spacing for Colorado and St Lawrence than the other regions to better illustrate the anomalies
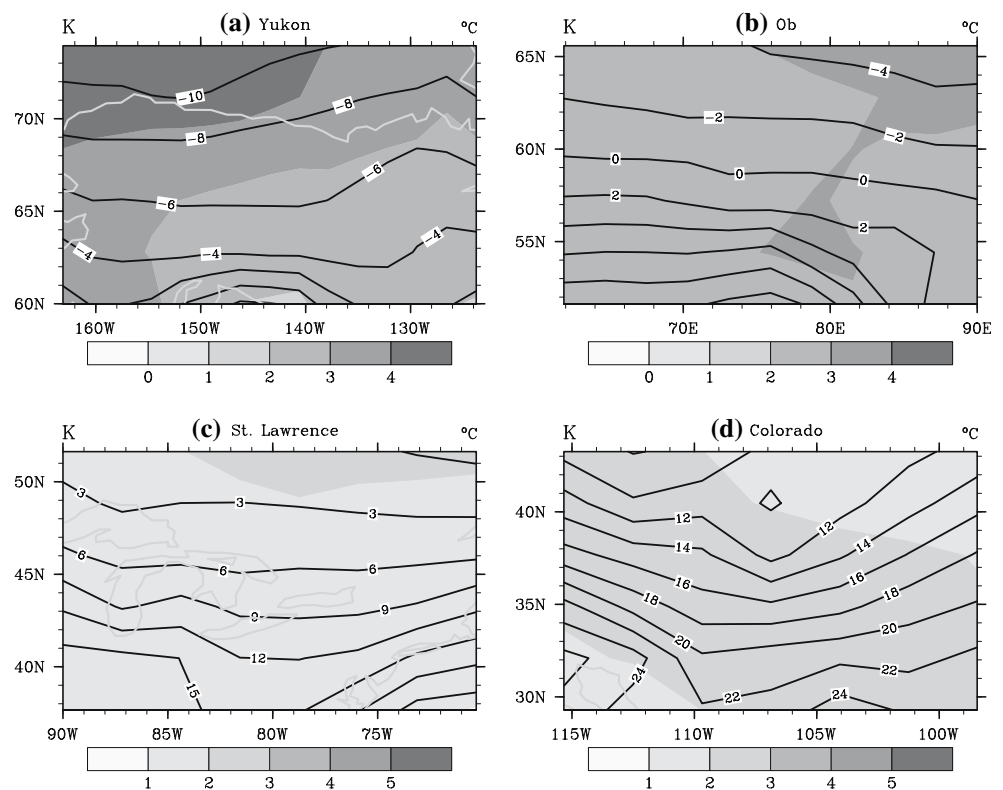
5 Interaction changes

Generally, moisture transport between hemispheres significantly increases year-round in response to doubled CO_2 (Fig. 10a), but in summer the increase of northward moisture transport exceeds the increase of southward transport. Net exchange of moisture between hemispheres significantly increases in boreal summer. These changes are important for interactions between any regional water cycle and the global water cycle.

In CTR and DBL, average monthly net moisture transport into the Arctic is minimum in May/June, when evapotranspiration is maximum. Thus, interaction between global and Arctic water cycles is weakest in May/June.

In response to doubled CO_2, the air is warmer and can hold more moisture before reaching saturation. Thus, compared to CTR, northward and southward moisture transport over the 60°N-latitude circle increases year-round in DBL, but net moisture transport changes only marginally (Fig. 10b).

In general, strong moisture flux through a region indicates great large-scale influence on the regional water cycle; weak moisture flux permits regional processes and/or conditions to influence or control the regional water cycle. In CTR the Yukon region shows the weakest interaction with the global water cycle. Annual moisture inflow and outflow nearly balance (Fig. 11a) amounting to approximately 1.62×10^4 kg m^{-2} mon^{-1} on annual average (Table 3). The Ob region has higher moisture inflow than

outflow through the year (Fig. 11b); annual moisture flux is 2×10^3 kg m^{-2} mon^{-1} higher in the Ob region than in the Yukon. Among our study regions, moisture flux is highest in the St Lawrence region (3.58×10^4 kg m^{-2} mon^{-1}); outflow exceeds inflow for most months (Fig. 11c), i.e., moisture from evapotranspiration within this region is exported. In the Colorado region, the surface divergence causes greater outflow than inflow from late fall to early summer (Fig. 11d).

In both climate scenarios, the Yukon, Ob, and St Lawrence regions are more influenced by the global water cycle in summer than winter; the opposite is true for the Colorado region (Fig. 11). Air in the Yukon, Ob, St Lawrence, and Colorado regions is appreciably moister (4.3, 5.8, 6.5, 2.6 g kg^{-1} respectively in CTR; 4.6, 6.0, 7.0, 2.7 g kg^{-1} in DBL) in summer than in winter. Average winds are also stronger in winter than summer for all study regions in both climate scenarios. In Colorado, however, the difference between summer and winter winds is greater than for other regions; moisture advection is higher in winter than summer. These results explain the observed difference between the Colorado region and the other regions in regional interactions with the global water cycle.

5.1 Yukon

In CTR, the Yukon region is governed by high pressure south of the region in summer, and low pressure (Aleutian

Fig. 9 Monthly averaged
residence time (ratio of domain-
averaged precipitable water to
domain-averaged precipitation)
from CTR (*solid*) and DBL
(*dashed*) for **a** global average,
b Yukon, **c** Ob, **d** St Lawrence,
and **e** Colorado. Note that
y-axes differ
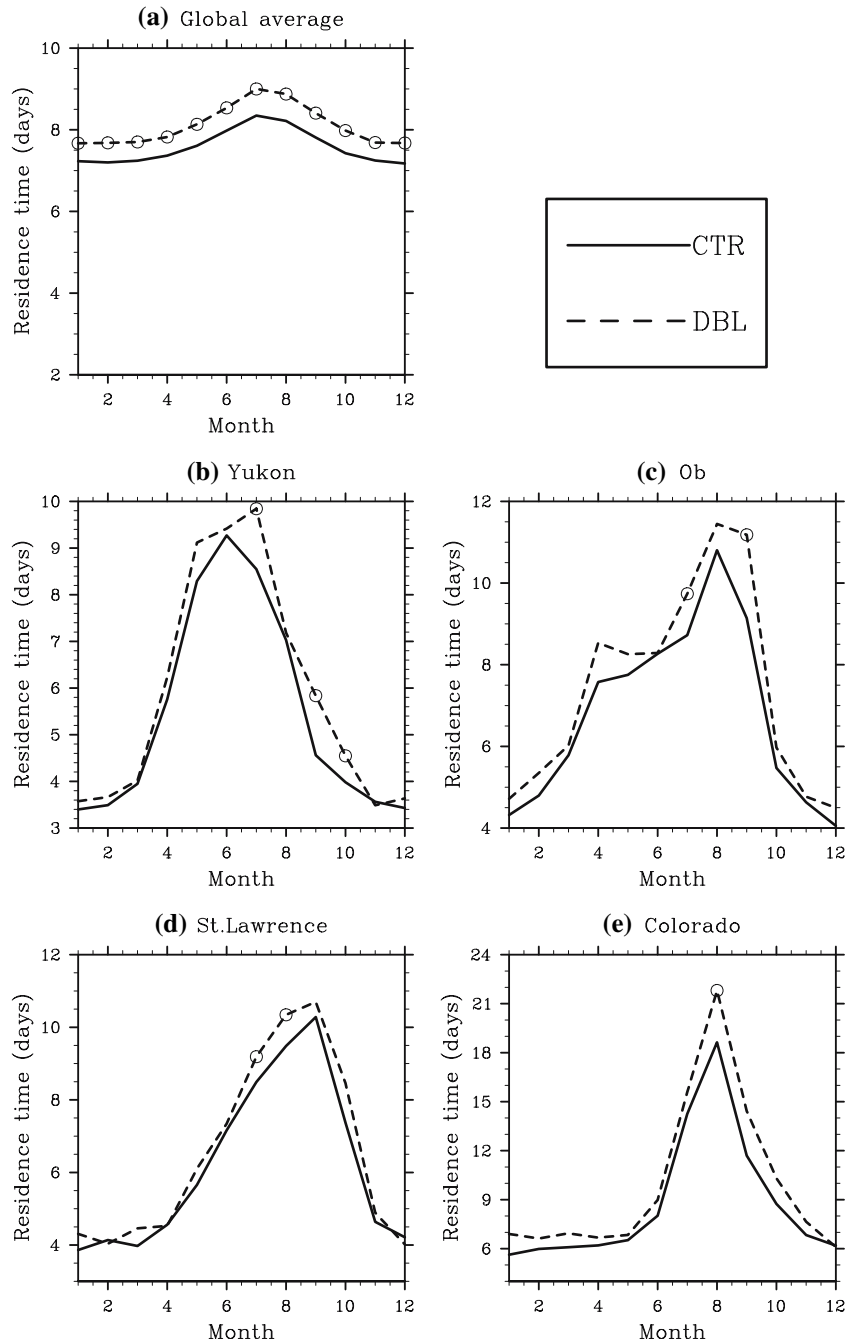
Low) in winter. Accordingly, in the southern Yukon, the prevailing near-surface wind direction changes from southeast (summer) to southwest (winter), and Pacific air penetrates further north into central Alaska in summer than winter (e.g., Fig. 12a).

In response to doubled CO$_2$, near-surface air temperatures are $\approx$5 K (2 K) higher in winter (summer) than under reference conditions. This greater winter temperature increase is commonly observed in high-latitude study regions, because of snow-albedo feedbacks and later snow

onset in DBL than CTR. Enhanced near-surface DBL air temperatures yield higher saturation vapor pressures and higher air moisture content than in CTR.

Doubling CO$_2$ causes a weakened winter Aleutian Low (4 hPa increase in the center) compared to CTR (Fig. 12b). In both scenarios in May, the Aleutian Low is centered near the Bering Strait; increased wind speed results in higher outflow than inflow at the western regional boundary. In August, the slightly northward-shifted center of the high-pressure system over the Bering Sea enhances

Table 2 Annual residence-time averages for control (CTR) and doubled CO$_2$ simulation (DBL), and percentage change (Δ = (DBL − CTR)·100/CTR); significant changes are bolded

	CTR (days)	DBL (days)	Δ (%)
Yukon	5.4	5.9	**9.2**
Ob	7.0	7.6	**8.9**
St Lawrence	6.2	6.6	**6.4**
Colorado	9.2	10.7	**16.3**
North of 60°N	6.3	6.9	**9.5**
Northern Hemisphere	8.0	8.6	**7.5**
Global	7.4	7.9	**6.7**

near-surface wind speed and moisture flux into the region from the Gulf of Alaska by $\leq 5 \times 10^3$ kg m^{-2} mon^{-1}.

In DBL, higher temperature and reduced Arctic Ocean and Bering Sea sea-ice cover enhance late fall/early winter water-vapor supply to the atmosphere. Increased temperature and water supply to the atmosphere over the Aleutians significantly increases moisture flux into the region in February and through the region in November (Fig. 11a); water supply to the atmosphere is increased because the area of ice-covered waters adjacent to the region is reduced.

Due to warmer DBL temperatures, evapotranspiration increases significantly in most months (Fig. 6b). Earlier snowmelt permits earlier transpiration onset in DBL than in CTR. Early summer evapotranspiration spatial variability increases significantly (based on the F-test; 3.2 mm mon^{-1}) due to increases in precipitation and its variability. In DBL, delayed snow-cover establishment and decreased sea-ice cover over the Arctic Ocean and Chukchi Sea largely contribute to increased early fall evapotranspiration.

Monthly precipitation increases significantly for more than half of the months (Fig. 4b). Increased DBL summer precipitation is due to increased moist convection. Summer air temperature increases more over land (2.2 K) than over

ocean (1.5 K) along the Gulf of Alaska, so increases in upward motion and convection in DBL are stronger over land than ocean. In August/September, in both DBL and CTR, the major source of precipitation is no longer convection, but advection from low-pressure Bering Sea weather systems. The low pressure centered over the Bering Sea deepens in response to doubling CO$_2$; coastal winds decrease by 0.7 m s^{-1} and less Gulf of Alaska moisture is transported into the region (Fig. 12c, d). Consequently, less September precipitation falls in DBL than in CTR due to reduced interaction of global and regional water cycles.

During spring, the ground is still frozen. Thus, in both scenarios, snowmelt contributes mainly to runoff rather than to soil moisture. In DBL, spring runoff peak occurs in May as in CTR, but starts earlier and diminishes more quickly as summer approaches (Fig. 7b). The runoff change results from decreased domain-averaged snowfall (2.3 mm mon^{-1}) and snow depth due to warmer conditions; precipitation falls as rain rather than snow more often in DBL than in CTR.

The February-to-April upper-soil frozen fraction is smaller in DBL than in CTR because of slightly increased soil temperatures. In the upper soil layer, total volumetric water content (liquid + ice) is lower in DBL than CTR from May to January, but higher from February to April (Fig. 13b); the increase occurs because precipitation more frequently occurs as rain, and snowmelt contributes to runoff with a slightly reduced fraction in DBL than CTR. Increased DBL evapotranspiration reduces soil volumetric water content from May onwards compared to CTR, despite precipitation increases during all months in DBL.

In summary, doubling CO$_2$ slightly enhances Yukon regional interactions with the global water cycle (net exchange increases by 14.8%; Table 3) leading to more regional precipitation that is not balanced by increased evapotranspiration; i.e., the Yukon loses influence over its

Fig. 10 Comparison of monthly averaged northward (*thin solid* for CTR; *thin dashed* for DBL) and southward (*thin dotted* for CTR; *thin dash-dotted* for DBL) moisture (water vapor + liquid and solid atmospheric water substances) fluxes and net (northward–southward) flux (*thick solid* for CTR; *thick dashed* for DBL) over the **a** equator, and **b** 60°N-latitude circle. *Circles squares, and stars* indicate significant (95% confidence level or higher) differences between DBL and CTR
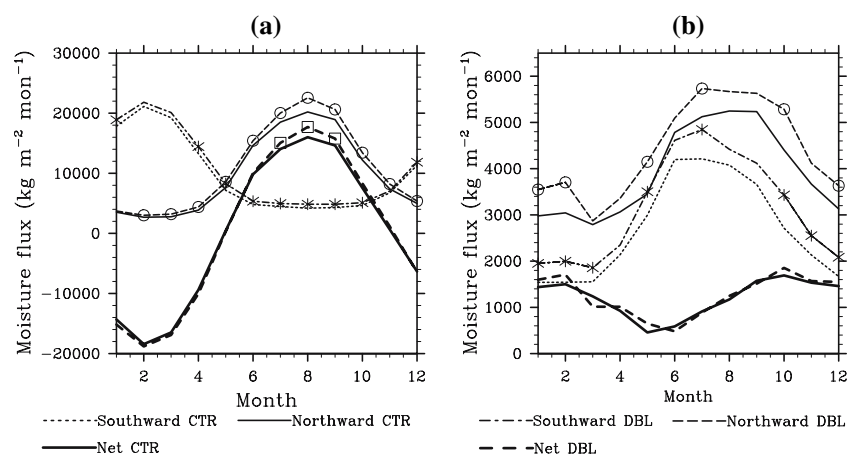
Fig. 11 Comparison of monthly averaged moisture fluxes over the lateral boundaries of **a** the Yukon, **b** the Ob, **c** the St Lawrence, and **d** the Colorado regions. Inflow and outflow in CTR are shown as *thin solid* and *thin dashed lines*, respectively; anomalies (DBL-CTR) of inflow and outflow are shown as *thick solid and thick dashed lines*, respectively. Significant (95% confidence level or higher) changes are indicated as *circles and squares*

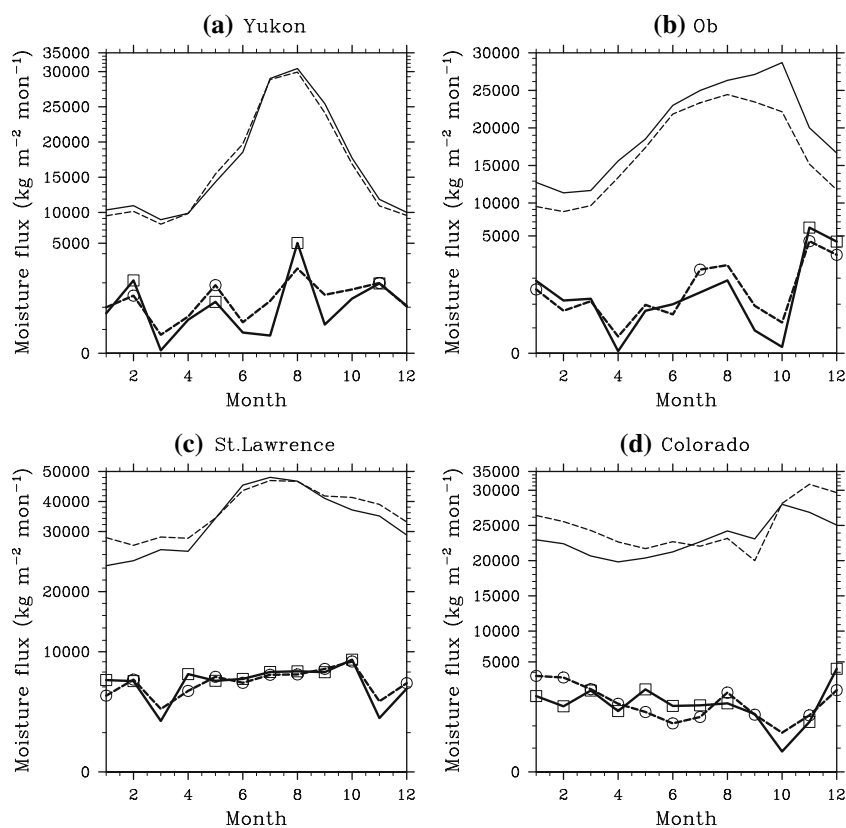**Table 3** Annual average of total water fluxes (kg m⁻² mon⁻¹) through the study domains for the control (CTR) and doubled-CO₂ (DBL) simulation, and percentage change (Δ = (DBL – CTR)·100/CTR); significant changes are bolded

	CTR	DBL	Δ (%)
Yukon	16,249	18,374	**14.8**
Ob	18,221	20,579	**14.8**
St Lawrence	35,796	40,723	**14**
Colorado	23,938	26,763	**12**
North of 60°N	3,305	3,770	10.3
Northern hemisphere	9,852	10,671	7.9

own regional water cycle, while upwind regions gain influence.

5.2 Ob

In CTR, interactions between regional and global water cycles differ between summer and winter. From April to August, the wind relaxes, and blows from the west or the north; from September to March southwesterly winds prevail. Thus, from April to August the Ob region receives little or no moisture advection from the Mediterranean Sea and/or Atlantic Ocean; local convection contributes more to precipitation than in other months (Fig. 14).

In DBL, November and December near-surface temperatures increase about 4 K; simultaneously, the Icelandic low deepens. Southwesterly winds and water-vapor transport from the Atlantic Ocean and Mediterranean Sea into Siberia is enhanced in DBL compared to CTR, and interactions of regional and global water cycles increase significantly during winter in DBL compared to CTR (Fig. 14b). In November and December, increased incoming and outgoing moisture flux reaches a maximum of $\approx 5 \times 10^3$ kg m⁻² mon⁻¹. Increased inflow slightly exceeds increased outflow (Fig. 11b) because November–December precipitation significantly increases in DBL, compared to CTR (Fig. 4c). The significant July outflow increase suggests enhanced surface divergence and moisture export from the Ob region to adjacent areas.

June precipitation increases significantly due to enhanced local convection triggered by higher surface temperatures and evapotranspiration in DBL than CTR (Figs. 5b, 8b). In the other months (except September–October), monthly averaged precipitation is slightly higher in DBL than in CTR (Fig. 4c).

Evapotranspiration increases significantly in all months in DBL (Fig. 6c), partly because DBL's warmer atmospheric conditions impose higher atmospheric demands, and partly because precipitation increases. Maximum increased annual evapotranspiration occurs in the Ob
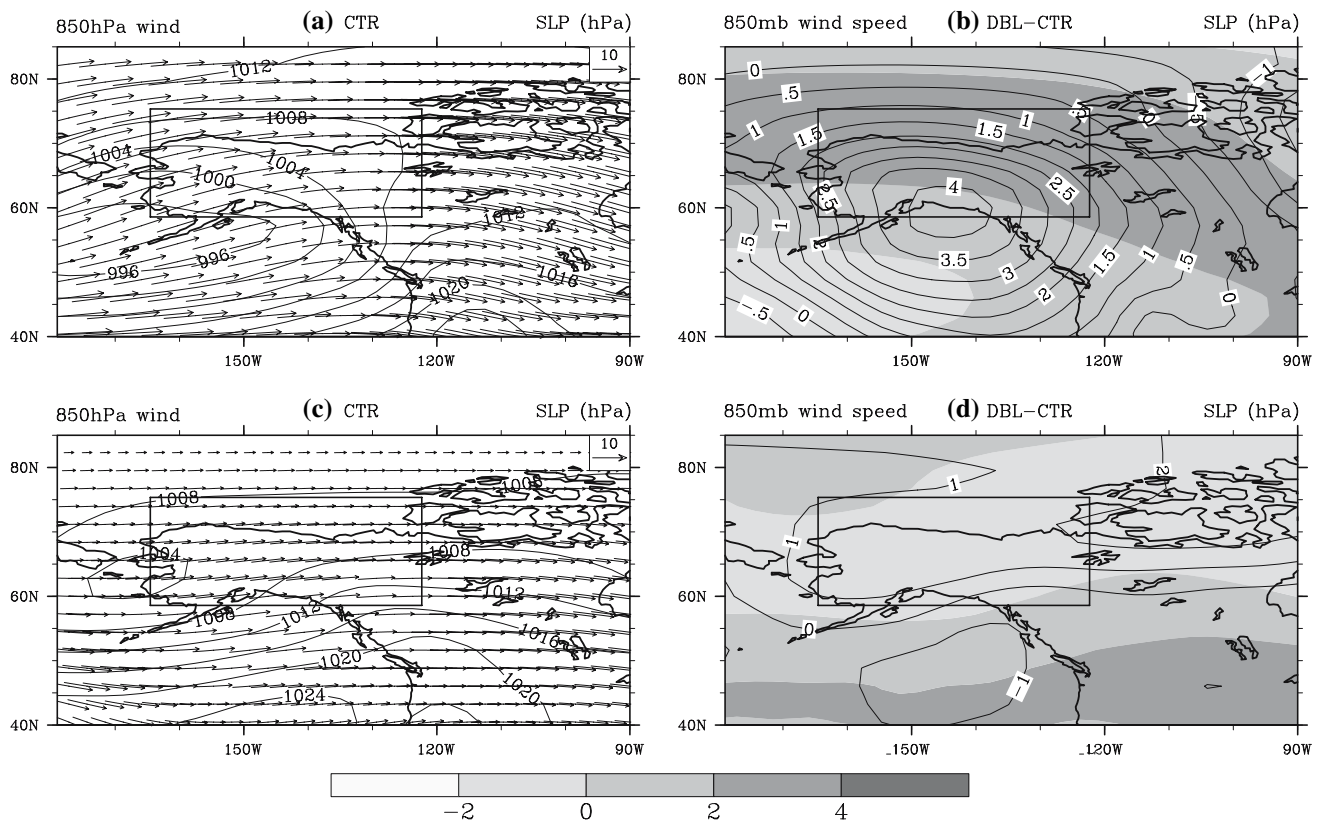
Fig. 12 Sea level pressure (in hPa) over the region defined by 40–85°N and 180–90°W as obtained in DJF for **a** CTR, **b** anomalies (DBL-CTR), and in September for **c** CTR, and **d** anomalies (DBL-CTR). The Yukon region is shown in the *box*. In part **b** and **d** *shaded regions* represent wind-speed magnitude differences at 850 hPa. In part **a** and **c** *arrows* are wind at 850 hPa

region center, where annual CTR evapotranspiration was already the highest. The spatial evapotranspiration standard deviation increases in most months; the changes reach significance in December–March. This higher spatial standard deviation and the DBL spatial pattern change are related to greater temperature and precipitation increases in the center than elsewhere in the Ob region, indicating again that altered evapotranspiration triggers precipitation variability.

Generally, winter soils are close to saturation in both CTR and DBL. Consequently, snowmelt mainly contributes to runoff rather than to increased soil moisture. In DBL the runoff peak is slightly reduced, but runoff volume is slightly higher in winter and early spring than in CTR (Fig. 7c). Altered runoff evolution results from slightly increased winter and early spring snowmelt rate. Under warmer DBL conditions temperatures above freezing occur more frequently than in CTR, so less snow remains for the melting season.

Upper soil moisture decreases in DBL compared to CTR year-round, with significant decreases in April, May, October, and November (Fig. 13c). These decreases are mainly due to enhanced evapotranspiration in summer,

responding to the higher DBL temperatures. Increased summer evapotranspiration exceeds increased precipitation.

In summary, in response to doubled CO_2 the Ob region, like the Yukon, experiences enhanced global water cycle interaction with ≈14.8% net water exchange increase. Moisture exports increase more strongly than imports; Ob impact on downwind regions is increased. Evapotranspiration and precipitation increases are similar.

5.3 St Lawrence

Similar to the Ob, the interaction between global and St Lawrence regional water cycles strongly differs between summer and winter. Under CTR, in winter this region is governed by a trough over the Great Lakes associated with a southwesterly flow; advected Great Lakes moisture is the major source of precipitation (Fig. 15a, b). In summer, the region is cut off from this moisture source because the high-pressure system over the subtropical North Atlantic Ocean moves northwestward. Winds are reduced compared to winter; local moist convection is the primary contributor to precipitation (Fig. 15c, d).

Fig. 13 Monthly average upper soil volumetric water content as obtained from CTR (*solid*) and DBL (*dashed*); **a** global, and **b** Yukon, **c** Ob, **d** St Lawrence, and **e** Colorado regions. Note that *y*-axes differ. *Circles* indicate significant changes
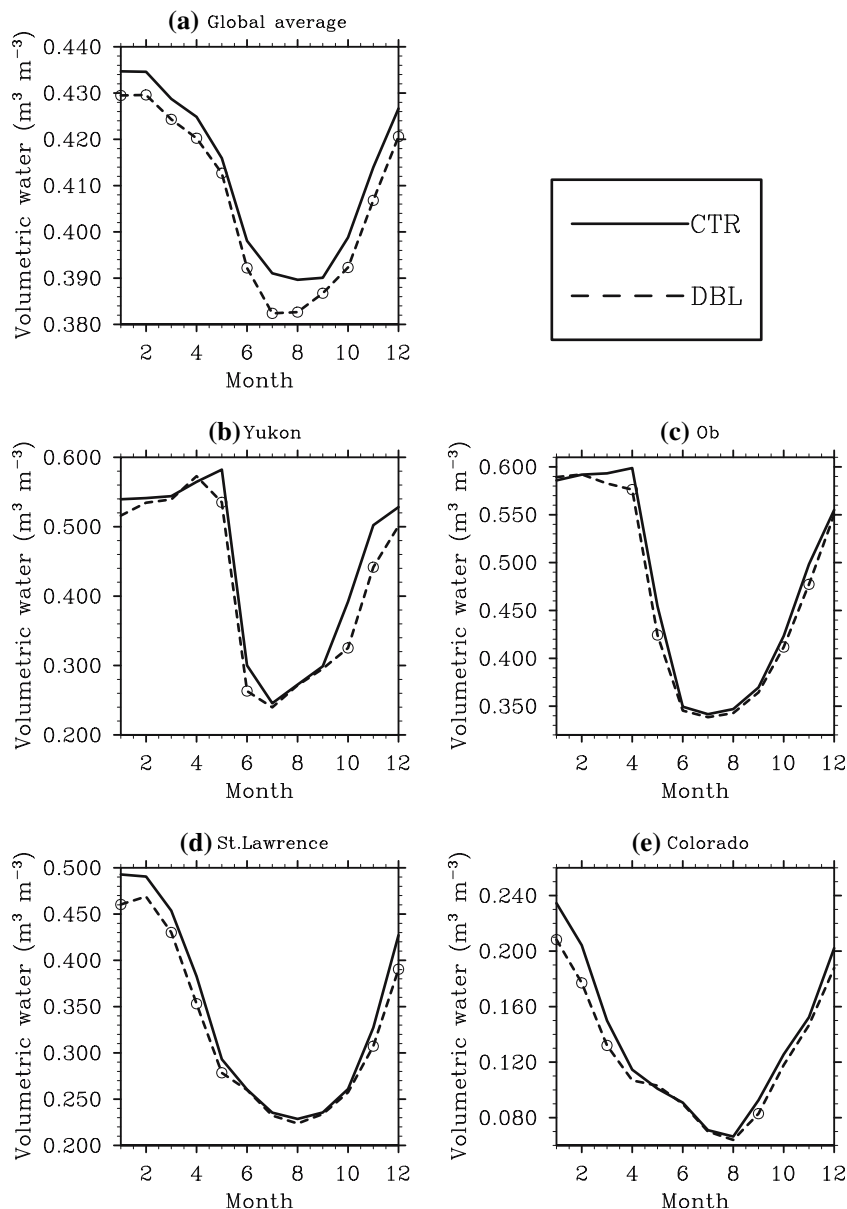
In CTR, slightly more atmospheric moisture leaves than enters the region from September to May (Fig. 11c), leading to annual average moisture export.

In DBL, moisture flux through this region increases significantly in all months except March and November (Fig. 11c). St Lawrence regional moisture flux increase is twice the increase in the other study regions; however, relative amounts are similar (Table 3). DBL inflow increases are slightly higher than outflow increases, suggesting increased global water cycle influence on this region. Nevertheless, the annual export and import cycles remain similar.

In DBL, precipitation increases in most months. April exhibits the largest change (Fig. 4d); changes are significant for April and December. Furthermore, the spatial precipitation variability greatly increases in summer and early winter. These changes can be explained as follows. A strengthened winter Icelandic Low and consequent deeper trough over the Great Lakes results in more precipitation from large-scale moisture advection in DBL than CTR (Fig. 15b). In DBL, increased summer evapotranspiration, especially increased evaporation over water surfaces (Great Lakes, Atlantic Ocean), leads to enhanced moist convection and hence increased precipitation compared to CTR.

Spatial patterns of high and low evapotranspiration differ marginally between CTR and DBL. Nevertheless, domain-averaged evapotranspiration is significantly higher year-round (Fig. 6d) due to increased precipitation and warmer temperature (+1.8 K annually) in DBL than in CTR.
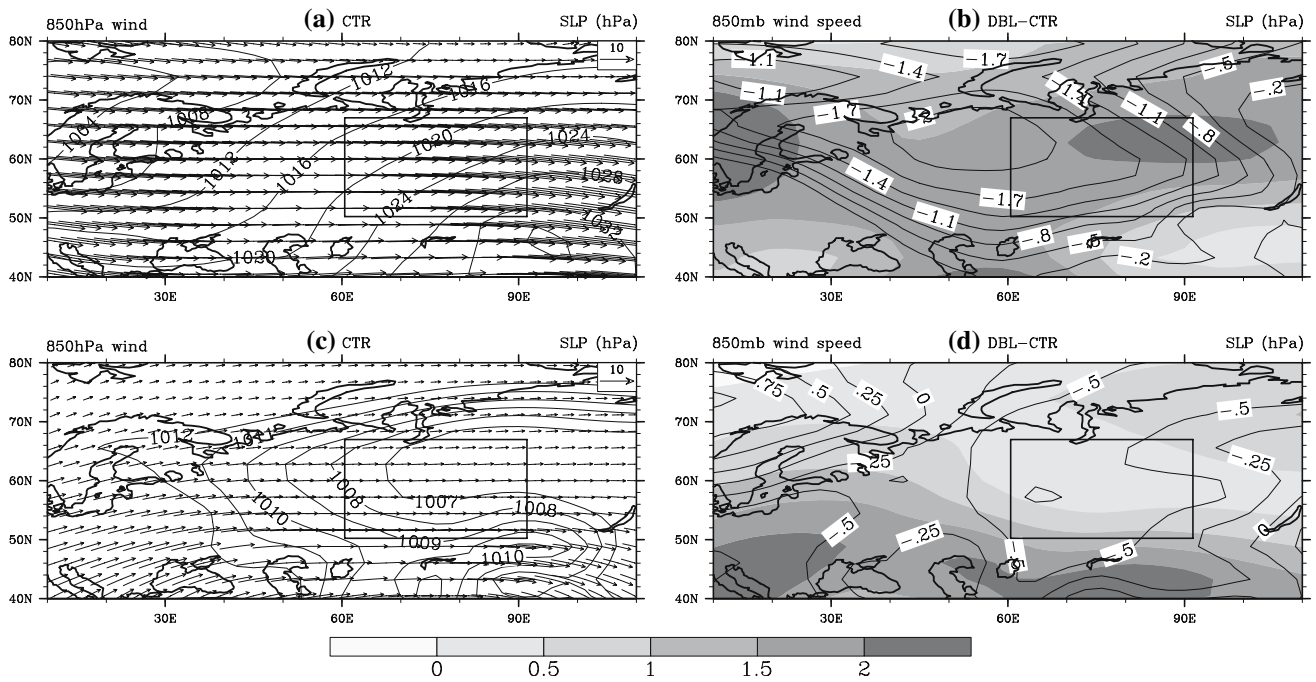
Fig. 14 Like Fig. 12, but sea-level pressure (in hPa) and anomalies (DBL-CTR) over the region defined by 40–80°N and 0–120°E as obtained in DJF for **a** CTR, **b** anomalies (DBL-CTR), and in JJA for **c** CTR, and **d** anomalies (DBL-CTR). The Ob region is shown in the *box*
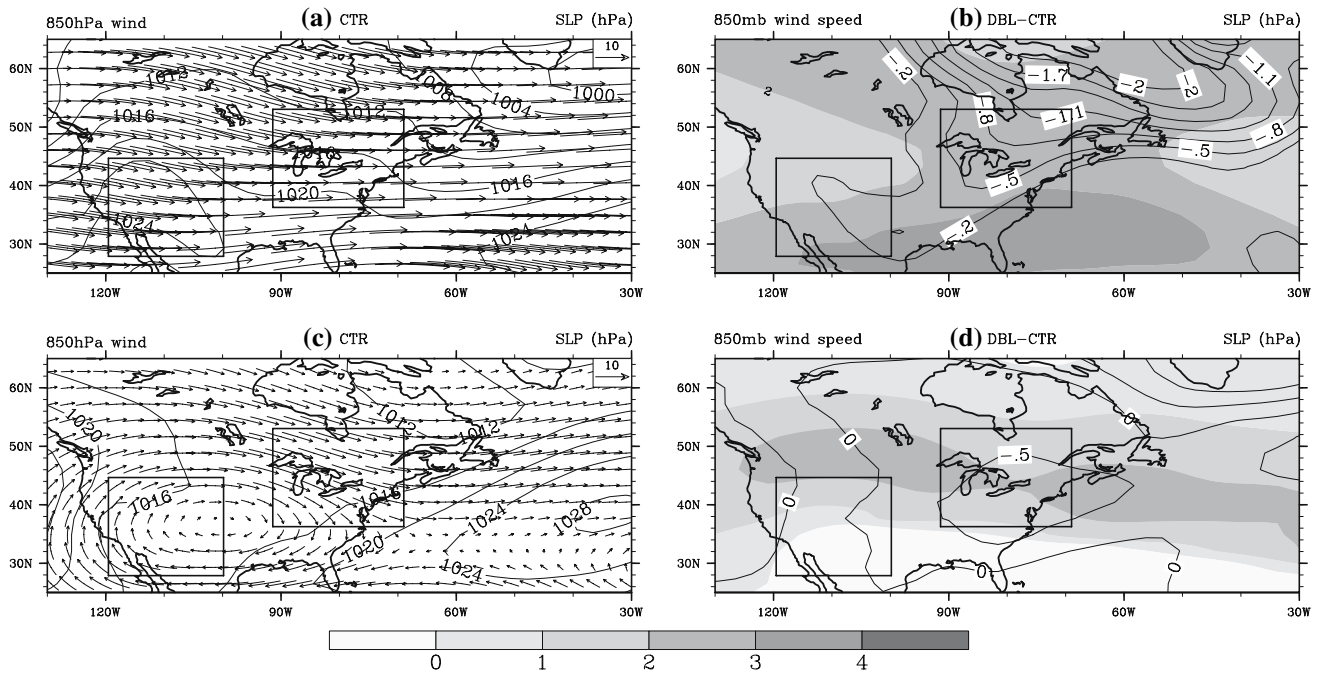

Fig. 15 Like Fig. 12, but sea-level pressure (in hPa) and anomalies (DBL-CTR) over the region defined by 25–65°N and 130–30°W as obtained in DJF for **a** CTR, **b** anomalies (DBL-CTR), and in JJA for **c** CTR, and **d** anomalies (DBL-CTR). The Colorado and St Lawrence regions are shown in the *left* and *right boxes*, respectively

In CTR and DBL, precipitation is greatest in summer. Nevertheless, summer runoff is low, because an appreciable amount of precipitation goes into evapotranspiration (Figs. 4d, 6d). In CTR runoff is increased by snowmelt, peaking in March. This peak shifts to April in DBL because the greatest precipitation increase occurs in April (Fig. 4d).

Compared to CTR, the DBL runoff peak is reduced because (1) snowmelt onset is earlier under warmer DBL conditions and (2) precipitation occurs less frequently as snow in DBL than in CTR. Winter runoff increases ≤4 mm mon^{-1} (Fig. 7d) because (1) more winter precipitation falls as rain in DBL, and (2) total (rain + snow) winter precipitation increases (Fig. 4d).

Increased evapotranspiration (Fig. 6d) leads to year-round decreased DBL total soil moisture; the winter and spring decrease is greatest. Soil moisture significantly decreases for most months from late fall to late spring (Fig. 13d); consequently, less regionally stored water is available in DBL than in CTR. Note that upper soil volumetric water content also decreases on global average (Fig. 13a).

In summary, precipitation increases slightly more than evapotranspiration, and annually averaged inflow increase exceeds outflow increase; under doubled CO_2 the global water cycle increases its influence on the St Lawrence regional water cycle and the St Lawrence loses influence over its downwind regions.

5.4 Colorado

In both CTR and DBL, the high pressure-system location changes slightly from summer to winter; interactions between regional and global water cycles differ slightly between winter and summer. Central Colorado-region wind-field divergence produces easterly (westerly) winds in the southern (northern) part of the domain. Therefore, regional outflow exceeds inflow from October to June (Fig. 11d). In summer, convergence occurs in the region's northeast. Moisture inflow is higher than outflow in July, August, and September (Fig. 11d), suggesting net regional moisture gain due to large-scale advection in both climate scenarios at this time of year.

In DBL, both moisture inflow and outflow increase significantly in all months except October (Fig. 11d). This increased summer interaction between global and Colorado regional water cycles is caused by increased near-surface wind (≤0.2 ms^{-1}) and increased air water-vapor content compared to CTR; during winter, increased interaction is due to increased moisture content.

From January to March and September to October, this region is governed by anti-cyclonic wind and downward motion on both sides of the Rocky Mountains in CTR and DBL. In DBL air temperatures are more than 2 K higher than in CTR, as is the saturation vapor pressure. Consequently, under the dry conditions and often anti-cyclonic circulation, high saturation deficits and consequently less precipitation occur more frequently in DBL than in CTR (Fig. 4e) as regional evapotranspiration (Fig. 6e) fulfills the atmospheric demands less frequently.

Overall, in DBL, monthly precipitation decreases compared to CTR, except in May and December. In May, precipitation increases southwest and northeast of this region. Enhanced coastal wind (≤0.49 ms^{-1}) transports warmer (≤2.8 K) and moister (≤0.6 g kg^{-1}) Pacific air into the Colorado region. As this flow encounters the Rocky Mountains, the orographically forced lifting of this relatively moister air mass leads to more upwind-side precipitation in DBL than in CTR. Note that here some uncertainty may be involved as the mountains are much "flatter" in CCSM than their highest peaks in nature. Simultaneously, the southerly flow advects more Gulf-of-Mexico moisture into the region in DBL than in CTR. This warm, moisture-rich flow and cold air advected from the high plains results in enhanced low-level moisture convergence and more precipitation in the region's northeast corner in DBL than in CTR, leading to ≥0.9 g kg^{-1} moister air. Thus, interactions between the global water cycle (enhanced Pacific Ocean and Gulf-of-Mexico moist warm air advection) and the regional water cycle (drainage of cold air from the High Plains) modify the May precipitation pattern. Increased December precipitation is due to advection of moister air, ≤0.8 g kg^{-1}, into the southern part of this region near the Gulf of California in DBL than in CTR. Again, the altered global water cycle affects the regional water cycle.

Soil moisture is low throughout the year, with an August minimum and a winter maximum (about 50% of saturation) (Fig. 13e). This annual cycle remains the same in DBL, but with slightly lower values. Despite potential evaporation increases in DBL, evapotranspiration marginally decreases ≤10% from April to September (Fig. 6e), because soil moisture limits evaporation even more in DBL than in CTR. In winter, despite drier soil in DBL than CTR, the soil is still wet enough to permit significantly increased evapotranspiration in response to higher (2 K) near-surface air temperatures (Fig. 6e).

Due to increased snow sublimation and decreased precipitation, annual accumulated runoff decreases in DBL (Table 4). In the annual cycle precipitation is slightly higher in DBL in May and December, so DBL runoff exceeds CTR runoff in these months (Figs. 4e, 7e).

In summary, under doubled-CO_2 conditions the global water cycle exerts increased influence over the Colorado regional water cycle.

6 Conclusions

Simulations with the fully coupled CCSM version 2.0.1 are performed with CO_2 concentrations of 355 ppm (control; CTR) and 710 ppm (experiment; DBL) to examine the impact of doubling CO_2 on global water cycle interactions

Table 4 Annual averages of accumulated precipitation, evapotranspiration, and runoff, and percentage changes (Δ = (DBL – CTR)·100/CTR) for the control (CTR) and doubled CO$_2$ (DBL) simulation; significant changes are bolded

	Precipitation				Evapotranspiration			Runoff		
	CTR (mm)	DBL (mm)	Δ (%)	GPCC (mm)	CTR (mm)	DBL (mm)	Δ (%)	CTR (mm)	DBL (mm)	Δ (%)
Yukon	563 (561)	620 (618)	**10.1 (10.2)**	(364)	175	202	**15.4**	224	231	3.1
Ob	542 (542)	578 (578)	**6.6 (6.6)**	(474)	379	409	**7.9**	124	122	–1.6
St Lawrence	863 (797)	914 (847)	**5.9 (6.3)**	(959)	742	778	**4.7**	147	145	–1.4
Colorado	503 (503)	496 (496)	–1.4 (–1.4)	(404)	413	415	**0.4**	70	63	–10
60°N	401 (389)	441 (430)	**10.0 (10.5)**	(307)	185	207	**11.3**	103	103	0
Northern Hemisphere	801 (660)	831 (695)	**3.7 (5.3)**	(661)	739	761	**3.0**	132	135	**2.3**
Global	840 (861)	861 (888)	**2.5 (3.1)**	(810)	773	789	**2.1**	131	134	**2.3**

Values in parentheses are for land-mass areas only, for comparison with the GPCC precipitation climatology

with regional water cycles of four similarly sized, but hydrologically and thermally different study regions (Yukon, Ob, St Lawrence, Colorado). A heuristic evaluation based on various published climatological data showed that, despite difficulties in accurately modeling annual high-altitude precipitation cycles and distribution, CCSM with 355 ppm CO$_2$ concentration generally produces acceptable results with respect to water-cycle-relevant quantities on monthly and annually averaged time scales and on global and regional spatial scales. Therefore, we conclude that CCSM describes water-cycle-relevant processes well, and is a suitable tool for examining the impact of doubling CO$_2$ on interactions between global and regional water cycles.

For all study regions, the annually averaged global water cycle interacts more strongly with the regional water cycle in DBL than in CTR (Table 3) for the following reasons: Increased temperatures mean increased saturated water-vapor pressure in DBL compared to CTR; warm air takes up more water vapor before saturation occurs and cloud and precipitation formation begins. Residence-time calculations show slowed regional water cycles under doubled CO$_2$, and indicate water vapor may be transported further from water sources. Thus in DBL, in principle, a region's potential radius of influence increases, but the region is also influenced by areas farther upwind than in CTR. The greatest increase (3.5 days) of residence time is found in the Colorado region where residence time is already the highest among the four study regions. In conclusion, increased residence time for the four regions indicates that their regional water cycles are more strongly influenced by outside regions in DBL than in CTR.

Annually averaged inflow increase exceeds outflow increase in the St Lawrence region in DBL; the opposite is true for the other study regions. This indicates potential changes in how regional water cycles interact with the global water cycle in a warmer climate. For regions with approximately equal moisture import and export under

CTR, such as the Yukon, doubling CO$_2$ establishes more balanced water inflow and outflow. For the Ob region, evapotranspiration and precipitation increases are nearly identical in response to doubled CO$_2$. In DBL, evapotranspiration increases much less than precipitation in St Lawrence, strongly diminishing the moisture export role of this region; St Lawrence loses influence over the water cycles of its downwind regions. These findings suggest that the degree and character of doubled CO$_2$ impact on global and regional water cycle interactions is regionally dependent.

Global and regional water cycle interactions are enhanced significantly in more months in mid-latitude than high-latitude study regions (cf. Fig. 11). Primarily, for a given temperature increase, saturation water-vapor pressure increases more for a higher than lower reference temperature. Thus, despite larger temperature increases at high-latitudes than at mid-latitudes, the high-latitude saturated vapor-pressure increase is less and therefore atmospheric water demand increases much more at mid-latitudes than at high-latitudes.

Moisture flux increases affect regional water-cycle components differently for the four study regions because (1) the position and strength of semi-permanent pressure systems over or adjacent to the regions differ, as do (2) their regional changes in response to doubling CO$_2$. For regions where precipitation depends greatly on large-scale advection (Yukon, Ob), increased moisture inflow leads to increased precipitation in DBL compared to CTR. For regions where local convection is an important determinant of summer precipitation (St Lawrence, Colorado), summer precipitation changes are mainly controlled by regional evapotranspiration changes. Consequently, doubled CO$_2$ may produce wetter conditions for the humid St Lawrence region, but may exacerbate water shortages in the semi-arid Colorado region. Generally speaking, doubling CO$_2$ increases global water cycle influence on regional water cycles; impacts on regional water-cycle components

(evapotranspiration, precipitation) are greater at high-latitudes than at mid-latitudes and greater in winter than in summer.

References

AchutaRao K, Covey C, Doutriaux C, Fionino M, Gleckler P, Philips T, Sperber K, Taylor K, Bader D (eds) (2004) An appraisal of coupled climate model simulations. Tech Rep UCRL-TR-202550, University of California, Lawrence Livermore National Laboratory, Livermore. http://www-pcmdi.llnl.gov/model_appraisal.pdf, pp 28–31

Baumgartner A, Reichel E (1975) The world water balance. Elsevier, Amsterdam, p 179

Blackmon M, Boville B, Bryan F, Dickinson R, Gent P, Kiehl J, Moritz R, Randall D, Shukla J, Solomon S, Bonan G, Doney S, Fung I, Hack J, Hunke E, Hurrell J, Kutzbach J, Meehl J, Otto-Bliesner B, Saravanan R, Schneider EK, Sloan L, Spall M, Taylor K, Tribbia J, Washington W (2001) The Community Climate System Model. Bull Am Meteorol Soc 82:2357–2376

Bonan GB (1998) The land surface climatology of the NCAR land surface model coupled to the NCAR community climate model. J Clim 11:1307–1326

Bonan GB, Oleson KW, Vertenstein M, Levis S, Zeng X, Dai Y, Dickinson RE, Yang ZL (2002) The land surface climatology of the Community Land Model coupled to the NCAR Community Climate Model. J Clim 15:3123–3149

Briegleb BP, Hunke EC, Bitz CM, Lipscomb WH, Holland MM, Schramm JL, Moritz RE (2004) The sea ice simulation of the Community Climate System Model, version two. NCAR Technical Note. NCAR TN-45+STR, p 34

Broecker WS (1997) Thermohaline circulation, the Achilles heel of our climate system: will man-made CO_2 upset the current balance? Science 278:1582–1588

Colle BA, Mass CF, Westrick KJ (2000) MM5 precipitation verification over the Pacific Northwest during the 1997–99 cool seasons. Wea Forecasting 15:730–744

Coquard J, Duffy PB, Taylor KE, Iorio JP (2004) Present and future surface climate in the western USA as simulated by 15 global climate models. Clim Dyn 23:455–472

Covey C, AchutaRao KM, Cubasch U, Jones P, Lambert SJ, Mann ME, Phillips TJ, Taylor KE (2003) An overview of results from the Coupled Model Intercomparison Project. Global Planet Change 37:103–133

Croley TE II, Quinn FH, Kunkel KE, Changnon SA (1998) Great Lakes hydrology under transposed climates. Clim Change 38:405–433

Cubasch U, Meehl GA, Boer GJ, Stouffer RJ, Dix M, Noda A, Senior CA, Raper S, Yap KS (2001) Projections of future climate change. In: Houghton JT, Ding Y, Griggs DJ, Noguer M, van der Linden PJ, Dai X, Maskell K, Johnson CA (eds) Climate change 2001: the scientific basis. Contribution of working Group I to the

third assessment report of the intergovernmental panel on climate change. Cambridge University Press, Cambridge, p 881

Dai A, Trenberth KE (2004) The diurnal cycle and its depiction in the community climate system model. J Clim 17:930–951

Dai Y, Zeng X, Dickenson RE, Backer I, Bonan GB, Bosilovich MG, Denning AS, Dirmeyer PA, Houser PR, Niu G, Oleson KW, Schlosser CA, Yang ZL (2003) The Common Land Model. Bull Am Met Soc 84:1013–1023

Dingman SL (1994) Physical hydrology. Prentice-Hall, New Jersey, p 575

Eltahir EAB, Bras RL (1996) Precipitation recycling. Rev Geophys 34:367–378

Flato GM, Boer GJ, Lee WG, McFarlane NA, Ramsden D, Reader MC, Weaver AJ (2000) The Canadian Centre for Climate Modelling and Analysis global coupled model and its climate. Clim Dyn 16:451–467

Folland CK, Rayner NA, Brown SJ, Smith TM, Shen SS, Parker DE, Macadam I, Jones PD, Jones NR, Nicholls N, Sexton DMH (2001) Global temperature change and its uncertainties since 1861. Geophys Res Lett 28:2621–2624

Førland EJ, Hassen-Bauer I (2000) Increased precipitation in the Norwegian Arctic: true or false? Clim Change 46:485–509

Frei C, Schär C (1998) A precipitation climatology of the Alps from high-resolution rain-gauge observations. Int J Climatol 18:873–900

Furevik T, Bentsen M, Drange H, Kindem IKT, Kvamstø NG, Sorteberg A (2003) Description and evaluation of the Bergen climate model: ARPEGE coupled with MICOM. Clim Dyn 21:27–51

Giorgi F, Hewitson B, Christensen JH, Hulme M, von Storch H, Whetton P, Jones RG, Mearns LO, Fu C (2001) Regional climate information evaluation and projections. In: Houghton JT, Ding Y, Griggs DJ, Noguer M, van der Linden PJ, Xiaoxu D (eds) Chapter 10, Climate Change 2001: The scientific basis, contribution of working group I to the third assessment report of the Intergovernmental Panel on Climate Change (IPCC). Cambridge University Press, Cambridge, UK, pp 583–638

Gregory KJ, Walling DE (1973) Drainage basin form and process. Wiley, New York, p 456

Hack J (1994) Parameterization of moist convection in the National Center for Atmospheric Research Community Climate Model (CCM2). J Geophys Res 99:5551–5568

Hennessy KJ, Gregory JM, Mitchell JFB (1997) Changes in daily precipitation under enhanced greenhouse conditions. Clim Dyn 13:667–680

Hinkel KM, Nelson FE, Klene AE, Bell JH (2003) The urban heat island in winter at Barrow, Alaska. Int J Climatol 23:1889–1905

Holland MM (2003) The north Atlantic oscillation-Arctic oscillation in the CCSM2 and its influence on Arctic climate variability. J Clim 16:2767–2781

Holland MM, Bitz CM, Hunke EC, Lipscomb WH, Schramm JL (2006) Influence of the sea ice thickness distribution on polar climate in CCSM3. J Clim 19:2398–2414

Houghton JT, Ding Y, Griggs DJ, Noguer M, van der Linden PJ, Dai X, Maskell K, Johnson CA (eds) (2001) Climate change 2001: the scientific basis. Contribution of working group 1 to the third assessment report of the Intergovernmental Panel on Climate Change. Cambridge University Press, Cambridge, pp 36–40

Hulme M, Osborn TJ, Johns TC (1998) Precipitation sensitivity to global warming: comparison of observations with HadCM2 simulations. Geophys Res Lett 25:3379–3382

Johns TC, Carnell RE, Crossley JF, Gregory JM, Mitchell JFB, Senior CA, Tett SFB, Wood RA (1997) The second Hadley Centre coupled ocean-atmosphere GCM: model description, spinup and validation. Clim Dyn 13:103–134

Jones PD, Hulme M (1996) Calculating regional climatic time series for temperature and precipitation: methods and illustrations. Int J Climatol 16:361–377

Kiehl JT, Gent PR (2004) The Community Climate System Model, version 2. J Clim 17:3666–3682

Larson LW, Peck EL (1974) Accuracy of precipitation measurements for hydrologic modeling. Water Resource Res 10:857–863

Mahfouf JF, Cariolle D, Royer JF, Geleyn JF, Timbal B (1994) Response of the MÉTÉO-FRANCE climate model to changes in CO_2 and sea surface temperature. Clim Dyn 9:345–362

Meehl GA, Boer GJ, Covey C, Latif M, Stouffer RJ (2000) The Coupled Model Intercomparison Project (CMIP). Bull Am Met Soc 81:313–318

Milly PCD (1991) Potential evaporation and soil moisture in general circulation models. J Clim 5:209–226

Narapusetty B, Mölders N (2005) Evaluation of snow depth and soil temperatures predicted by the hydro-thermodynamic soil-vegetation scheme coupled with the fifth-generation Pennsylvania State University-NCAR mesoscale model. J App Met 44:1827–1843

National Climatic Data Center (1987) Monthly climatic data for the world, vol 40, nos. 1 and 7. NOAA, NCDC, Asheville

Oliver JE, Fairbridge RW (1987) The encyclopedia of climatology. Van Nostrand, Reinhold, New York, p 500

Peterson TC, Vose RS (1997) An overview of the global historical climatology network temperature data base. Bull Am Met Soc 78:2837–2849

Rasch PJ, Kristjánsson JE (1998) A comparison of the CCM3 model climate using diagnosed and predicted condensate parameterizations. J Clim 11:1587–1614

Smith RD, Dukowicz JK, Malone RC (1992) Parallel ocean general circulation modeling. Physica D 60:38–61

Su F, Adam JC, Trenberth KE, Lettenmaier DP (2006) Evaluation of surface water fluxes of the pan-Arctic land region with a land surface model and ERA-40 reanalysis. J Geophys Res 111:D05110. doi:10.1029/2005JD006387

Uppala SM, Kållberg PW, Simmons AJ, Andrae U, da Costa Bechthold V, Fiorino M, Gibson JK, Haseler J, Hernandez A, Kelly GA, Li X, Onogi K, Saarinen S, Sokka N, Allan RP, Anderson E, Arpe K, Balmaseda MA, Beljaars ACM, van de Berg L, Bidlot J, Bormann N, Caires S, Chevallier F, Dethof A, Dragosvac M, Fisher M, Fuentes M, Hagemann S, Hólm E, Hoskins BJ, Isaksen L, Janssen PAEM, Jenne R, McNally AP, Mahfouf J-F, Morcette J-J, Rayner NA, Saunders RW, Simon P, Sterl A, Trenberth KE, Untch A, Vasiljevic D, Viterbo P, Woollen J (2005) The ERA-40 re-analysis. Quart J Meterol Soc 131:2961–3011

Wang M, Liu Q, Yang X (2004) A review of research of human activity induced climate change. I. Greenhouse gases and aerosols. Adv Atmos Sci 21:314–321

Yang D, Goodison BE, Metcalfe JR, Golubev VS, Bates R, Pangburn T, Hanson CL (1998) Accuracy of NWS 8" standard nonrecording precipitation gauge: results and application of WMO intercomparison. J Atmos Oceanic Technol 15:54–68

Yang D, Woo MK (1999) Representativeness of local snow data for large scale hydrologic investigations. Hydrol Process 13:1977–1988

Zhang GJ, McFarlane NA (1995) Role of convective scale momentum transport in climate simulation. J Geophys Res 100:1417–1426

Zhang GJ, Kiehl JT, Rache PJ (1998) Response of climate simulation to a new convective parameterization in the National Center for Atmospheric Research Community Climate Model (CCM3). J Clim 11:2097–2115

Zhang MH, Lin W, Bretherton CS, Hack JJ, Rasch PJ (2003) A modified formulation of fractional stratiform condensation rate in the NCAR community atmospheric model CAM2. J Geophys Res 108(D1):4035. doi:10.1029/2002JD002523

Zhong S, In HJ, Bian X, Charney J, Heilman W, Potter B (2005) Evaluation of real-time high-resolution MM5 predictions over the Great Lakes region. Mon Wea Rev 20:63–81